




Role of isotopes in microturbulence from linear to saturated Ohmic confinement regimes

Lei Qi ^{*}, Jae-Min Kwon, T. S. Hahm, M. Leconte , Sumin Yi , Y. W. Cho, and Janghoon Seo
Korea Institute of Fusion Energy, Daejeon 169-148, South Korea



(Received 25 April 2023; accepted 27 November 2023; published 8 January 2024)

The first-principle gyrokinetic numerical experiments investigating the isotopic dependence of energy confinement achieve a quantitative agreement with experimental empirical scalings, particularly in Ohmic and L-mode tokamak plasmas. Mitigation of turbulence radial electric field intensity $|\delta E_r|^2$ and associated poloidal $\delta \mathbf{E} \times \mathbf{B}$ fluctuating velocity with the radial correlation length $l_{cr} \propto M_i^{0.11}$ strongly deviating from the gyro-Bohm scaling is identified as the principal mechanism behind the isotope effects. Three primary contributors are classified: the deviation from gyro-Bohm scaling, zonal flow, and trapped electron turbulence stabilization. Zonal flow enhances isotope effects primarily through reinforcing the inverse dependence of turbulence decorrelation rate on isotope mass with $\omega_c \propto M_i^{-0.76}$, which markedly differs from the characteristic linear frequency. The findings offer insights into isotope effects, providing critical implications for energy confinement optimization in tokamak plasmas.

DOI: [10.1103/PhysRevResearch.6.L012004](https://doi.org/10.1103/PhysRevResearch.6.L012004)

Deuterium (D) and tritium (T), pivotal to fusion energy, serve as the fuel for power generation in fusion plants, making their reactor-level operation a crucial objective for ITER [1]. Experiments across various tokamaks show that isotopes enhance energy confinement, epitomized by a general empirical scaling $\tau_E \propto M_i^\sigma$, where τ_E denotes energy confinement time, and M_i represents isotope mass ratio to hydrogen. σ varies between 0.2 and 0.5 [2–8] in nearly all operation regimes across worldwide tokamaks. Compiling data from diverse tokamaks, differing in size and magnetic configurations, L-mode confinement scaling ITER89-P [9] indicated $\sigma = 0.5$, and H-mode confinement scaling ITER-IPB(y) [4] yielded $\sigma = 0.2$. Intriguingly, isotopic dependence in Ohmic plasmas on ASDEX revealed $\sigma = 0.31$ in the low-density linear Ohmic confinement (LOC) regime and $\sigma = 0.5$ in the high-density saturated Ohmic confinement (SOC) regime [2]. Further, recent experiments shed light on the influence of isotopes on L-H power threshold in DIII-D [10], pedestal height in JET [11] and ASDEX Upgrade [7]. Given these findings, it is pivotal to unravel isotope effects in less complex plasma states like Ohmic and L-mode.

Despite experimental findings, theoretical understanding of isotope effects remains poor and constitutes a conundrum to date. Mixing-length diffusivity, $\chi_{ML} \sim \gamma/k_\perp^2$, scales as $\propto M_i^{0.5}$ from the gyro-Bohm scaling with perpendicular wave number $k_\perp \propto M_i^{-0.5}$. Similarly, gyro-Bohm diffusivity $\chi_{GB} = \rho_i^2 V_{Ti}/a$ exhibits a proportional relationship with $M_i^{0.5}$.

These predict a scaling $\tau_E \propto 1/\chi \propto M_i^{-0.5}$ at odds with experimental findings. Here, γ represents linear growth rate, ρ_i is ion gyro radius, $V_{Ti} = \sqrt{T_i/M_i}$ denotes ion thermal velocity, and a refers to tokamak minor radius. Previous studies explored nonlinear regimes, with a particular focus on zonal flow [12], along with collisions [13], electromagnetic effects [14], nonadiabatic electrons [15–18], and heating sources [19]. However, the scopes of these studies were limited, leading to incomplete understandings of isotope effects and shortage of consistent comparisons with experiments. To our knowledge, only qualitative consensus between experiments and theoretical models or simulations was attained in restricted regimes, illustrating that the pursuit of quantitative correlations is a significant challenge.

There has been a consistent need to elucidate the changes in energy confinement as density escalates, transitioning from the linear growth regime (LOC) to the saturated regime (SOC) in Ohmic and L-mode plasmas. Recent gyrokinetic simulations adeptly mirrored this LOC-SOC transition, depicting the shift in microturbulence dominance from trapped electron mode (TEM) to ion temperature gradient mode (ITG) due to stabilization of TEM by electron-ion collisions [20]. In this Letter, using state-of-the-art gyrokinetic numerical experiments, we illustrate the isotopic dependence of energy confinement, showing $\sigma \simeq 0.5$ at the low-density LOC regime and $\sigma \simeq 0.25$ at the high-density SOC regime. This aligns quantitatively with empirical scalings with σ ranging from 0.2 to 0.5. Additionally, we introduce a groundbreaking mechanism that explicates isotope effects driving this quantitative correlation. The mechanism stands out to replicate experimental observations of advantageous isotopic dependence of energy confinement, evident during LOC-SOC transition across multiple tokamaks, including ASDEX [2], JET-ILW [21], FT-2 [22], and TCV [23]. Our findings emphasize the pivotal role of isotopes in alleviating fluctuations of radial electric field $|\delta E_r|^2$ and associated poloidal $\delta \mathbf{E} \times \mathbf{B}$ flows.

^{*}qileister@kfe.re.kr

Radial correlation length $l_{cr} \propto M_i^{0.11}$ significantly deviates from the gyro-Bohm scaling, indicating three key factors behind isotope effects: deviation from the gyro-Bohm scaling, zonal flow, and stabilization of TEM.

In this work, we employ the δf version of cutting-edge first-principle global gyrokinetic particle-in-cell simulation platform gKPSP to conduct numerical experiments. In the code, ions are governed by gyrokinetic equations [24,25]. Bounce-averaged kinetics [26] is applied to describe trapped electrons with drift-kinetic passing electrons passively responding to fluctuations. Code details can be acquired in previous publications [27,28]. The code has been demonstrated capable to study ion-scale microturbulence with general tokamak geometry [29,30]. Simulations adopt parameters representative in typical Ohmic and L-mode discharges. Ion and electron density gradient is $R/L_{ni} = R/L_{ne} = 2.5$, electron temperature gradient is $R/L_{Te} = 7.5$, and ion temperature gradient is $R/L_{Ti} = 4.5$, wherein $L_x = -(d \ln x / dr)^{-1}$. Gradient profiles are given by the function $G(\varepsilon) = -\frac{R}{L_e} \exp\{-(\varepsilon - \varepsilon_c)/\varepsilon_\Delta\}^{20}$. Here, inverse aspect ratio $\varepsilon = r/R$ with r the radius; R/L_e represents normalized gradient; $\varepsilon_c = 0.18$ and $\varepsilon_\Delta = 0.054$ are the gradient profile's center and width, respectively. Ion and electron temperatures at the plasma center are $T_{i0} = 2.725$ keV and $T_{e0} = 5.5$ keV. Density at the plasma center n varies from $0.5 \times 10^{19} \text{ m}^{-3}$ to $9.0 \times 10^{19} \text{ m}^{-3}$. The safety factor is set up by $q = 0.58 + 3.04\varepsilon + 8.5\varepsilon^2$. Other main parameters are as follows: $a = 0.67$ m, major radius $R = 1.86$ m, and magnetic field $B_0 = 1.91T$. Maximum toroidal mode number $n_{\max} = 116$, which ensures $k_\theta \rho_i \sim 1.0$, covering both ITG and TEM regimes. Radial domain size $\rho^{*-1} = a/\rho_{iH} = 220$, with ρ_{iH} being hydrogen gyro-radius. A concentric circular tokamak geometry is applied, while for some cases shaped geometry with elongation $\kappa = 1.5$ is utilized. Coulomb collision operator is utilized for ion-ion collision, while electron-ion collision is modeled by the Lorentz pitch-angle scattering operator. Parameters considered here are in the low-collision regime.

Effective thermal energy transport diffusivity χ_{eff} is defined by Eq. (1), with $\chi_{e(i)}$ being electron (ion) heat transport diffusivity and $D_{e(i)}$ electron (ion) particle flux diffusivity. χ_{eff} is normalized to hydrogen gyro-Bohm diffusivity $\chi_{GBH} = \rho_{iH}^2 V_{TiH} / a$, with V_{TiH} being hydrogen thermal velocity. Thermal energy confinement time is calculated by $\tau_{\text{eff}} = a^2 / \chi_{\text{eff}}$ and displayed in Fig. 1(a) in terms of densities. Cases with zonal flow (w ZF) are indicated with symbols and solid lines, while scenarios without zonal flow (wo ZF) are indicated with only symbols. Open circles represent cases in shaped tokamak geometry with elongation $\kappa = 1.5$. Top axis indicates electron-ion effective collisionality $\nu_{ei}^* = \nu_{ei}^{\text{eff}} / \omega_{be}$ only for Fig. 1(a), and $\nu_{ei}^{\text{eff}} = \nu_{ei} / \varepsilon$. ν_{ei} is electron-ion collision frequency, and $\omega_{be} = V_{Te} / (qR_0 \varepsilon^{-1/2})$ is electron bounce frequency with $V_{Te} = \sqrt{T_e / m_e}$ being electron thermal velocity.

$$\chi_{\text{eff}} = \frac{\chi_e n_e \frac{\partial T_e}{\partial r} + \chi_i n_i \frac{\partial T_i}{\partial r} + D_e T_e \frac{\partial n_e}{\partial r} + D_i T_i \frac{\partial n_i}{\partial r}}{n_e \frac{\partial T_e}{\partial r} + n_i \frac{\partial T_i}{\partial r} + T_e \frac{\partial n_e}{\partial r} + T_i \frac{\partial n_i}{\partial r}} \quad (1)$$

Figure 1(a) highlights the following key aspects: (i) χ_{eff} undergoes a transition from the linear regime (LOC) at low density to the saturated regime (SOC) at high density, with

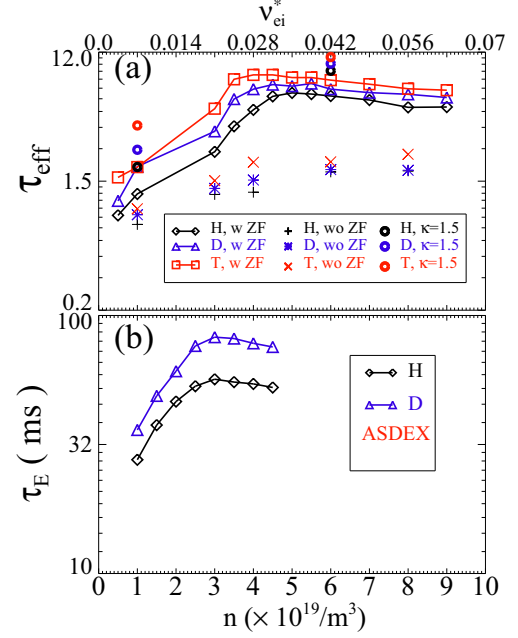


FIG. 1. (a) τ_{eff} is depicted against density n with (w ZF) and without (wo ZF) zonal flow, for H, D, and T. Open circles represent cases in shaped geometry with elongation $\kappa = 1.5$. Top axis indicates effective electron-ion collisionality ν_{ei}^* , and y axis is in log scale. (b) Energy confinement time adapted from Fig. 1(b) in Ref. [2].

isotopes leading to energy confinement improvement. This demonstrates fair agreement with the experimental trend shown in Fig. 1(b), adapted from Fig. 1(b) in Ref. [2]. Dots and lines represented in this figure are approximate mean values of scattered points in Fig. 1(b) of Ref. [2]. This observation remains consistent in shaped tokamak geometry with elongation $\kappa = 1.5$. (ii) Removal of zonal flow leads to degradation of confinement in all cases. Further analysis shows that zonal flow enhances isotope effects.

To decipher the underlying mechanism, we explore the characteristics of inherent turbulence. We employ Eq. (2) to scrutinize turbulence potential spectrum, which allows us to establish the potency of ITG and TEM $S_{\text{ITG-TEM}}$. Simulations illustrate that ITG is characterized by $\omega > 0$, $k_\theta > 0$, while TEM is identified with $\omega < 0$, $k_\theta > 0$. Dominance by ITG and TEM is indicated by positive and negative values of $S_{\text{ITG-TEM}}$, respectively, with ω symbolizing turbulence frequency, k_θ signifying poloidal wave number, and ϕ representing electrostatic potential. Figure 2 visualizes $S_{\text{ITG-TEM}}$ against density, color-coding hydrogen (black), deuterium (blue), and tritium (red) with symbols and solid lines. The graphical representation reveals a shift in turbulence dominance from TEM to ITG as density escalates. This aligns with prior gyrokinetic simulations which suggest TEM dominance in LOC and ITG dominance in SOC [31,32].

$$S_{\text{ITG-TEM}} = \frac{S_{\text{ITG}} - S_{\text{TEM}}}{S_{\text{tot}}} = \frac{\sum_{\omega > 0, k_\theta > 0} |\phi(\omega, k_\theta)| - \sum_{\omega < 0, k_\theta > 0} |\phi(\omega, k_\theta)|}{\sum_{\omega > 0, k_\theta > 0} |\phi(\omega, k_\theta)| + \sum_{\omega < 0, k_\theta > 0} |\phi(\omega, k_\theta)|} \quad (2)$$

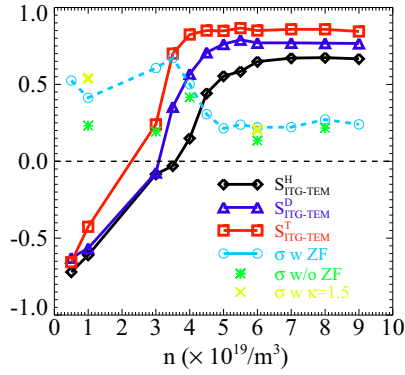


FIG. 2. ITG-TEM turbulence strength coefficient $S_{\text{ITG-TEM}}$ in terms of density for H, D, and T. σ is also depicted by open circles and dash line for scenarios with zonal flows (w ZF), discrete green * for scenarios without zonal flows (w/o ZF), and discrete \times for shaped cases with $\kappa = 1.5$.

We apply power law scaling $\tau_{\text{eff}} \propto M_i^\sigma$ for three isotopes under identical densities. Figure 2 showcases σ values at diverse densities. It is noteworthy that in the low-density (LOC) TEM dominant regime $\sigma \approx 0.5$, and $\sigma \approx 0.25$ in the high-density (SOC) ITG dominant regime, as summarized in Table I. Notably, a quantitative agreement between numerical and experimental data is attained with σ in the range from 0.2 to 0.5, evident when comparing to empirical data from ASDEX [2], ITER89-P scaling for L-mode [9], and ITER-IPB98(y) scaling for H-mode [4], as displayed in Table I. ITER89-P and ITER-IPB98(y) encompass data bases from diverse worldwide tokamaks with varying sizes and magnetic configurations, highlighting their general properties. The quantitative consensus is robust across a wide range of parameters for varying densities, elongations, radial domain sizes (ρ^{*-1}), and plasma profiles. An additional profile scan demonstrates that ITG turbulence with $R/L_n = 2$, $R/L_{Ti} = 6$, $R/L_{Te} = 2$, $n = 1.0 \times 10^{19}/\text{m}^3$ produces $\sigma = 0.22$, and TEM turbulence with $R/L_n = 2$, $R/L_{Ti} = 2$, $R/L_{Te} = 6$, $n = 1.0 \times 10^{19}/\text{m}^3$ yields $\sigma = 0.36$. When compared closely to ASDEX, our simulations highlight a more distinct isotope effect at lower densities. It is important to mention that our simulations do not exactly mirror plasma parameters found in ASDEX. Experimental settings are inherently more intricate with multiple varying parameters. As depicted in Fig. 1(a) of Ref. [2], electron temperature displays a pronounced shift from low to high density. Furthermore, in the low-density LOC regime, confinement time sees a rapid increase with density. This results in considerable shifts in σ even with minor variations in density measurements. For cases devoid of zonal flow, σ is represented by discrete green *.

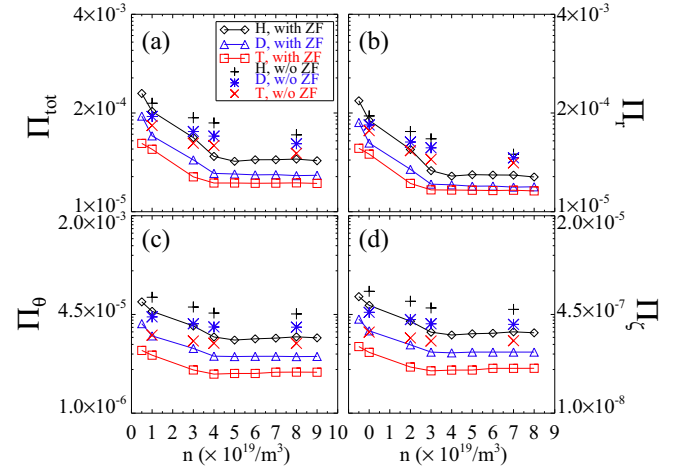


FIG. 3. (a) Π_{tot} , (b) Π_r , (c) Π_θ , and (d) Π_ζ are displayed versus n with (with ZF) and without zonal flow (w/o ZF), for H, D, and T. The y axis is in log scale.

zonal flow cases reveals that zonal flow boosts the isotopic dependence of energy confinement by escalating σ .

To deepen our understanding, it is crucial to delve into the turbulence spectrum [33–35] in three-dimensional (3D) tokamak geometry. We consequently define four forms of turbulence energy: total energy $\Pi_{\text{tot}} = \Pi_r + \Pi_\theta + \Pi_\zeta$, radial $\Pi_r = |\delta E_r|^2 = \sum_{k_r, k_\theta, k_\zeta} k_r^2 |\phi(k_r, k_\theta, k_\zeta)|^2$, poloidal $\Pi_\theta = |\delta E_\theta|^2 = \sum_{k_r, k_\theta, k_\zeta} k_\theta^2 |\phi(k_r, k_\theta, k_\zeta)|^2$, and toroidal $\Pi_\zeta = |\delta E_\zeta|^2 = \sum_{k_r, k_\theta, k_\zeta} k_\zeta^2 |\phi(k_r, k_\theta, k_\zeta)|^2$ electric field energies. Notably, radial electric field energy correlates with poloidal $\delta \mathbf{E} \times \mathbf{B}$ fluctuating velocity, and vice versa. Π_{tot} , Π_r , Π_θ , and Π_ζ are presented in Fig. 3. The figure clearly underscores that isotopes suppress radial, poloidal, and toroidal electric field energy, a pattern independent of zonal flow.

We proceed by calculating radial correlation length $l_{cr} = 2\pi/\bar{k}_r$, poloidal correlation length $l_{c\theta} = 2\pi/\bar{k}_\theta$, and eddy turnover rate $\omega_T \propto k_\theta \phi$. Here, $\bar{k}_r \equiv \sqrt{\Pi_r / \sum_{k_r, k_\theta, k_\zeta} |\phi(k_r, k_\theta, k_\zeta)|^2}$ and $\bar{k}_\theta \equiv \sqrt{\Pi_\theta / \sum_{k_r, k_\theta, k_\zeta} |\phi(k_r, k_\theta, k_\zeta)|^2}$. We also calculate decorrelation rate, $\omega_c = 2\pi/t_c$, using an alternative method. We compute autocorrelation of $\phi(t)$ at $11 \times 16 \times 11$ selected locations (radial \times poloidal \times toroidal), evenly spread across the 3D turbulence regime. t_c is then derived as the time distance from $t = 0$ to where the autocorrelation coefficient equals 0.5 and is averaged over all selected positions. We examine cases $n = [1.0, 3.0, 6.0, 8.0] \times 10^{19}/\text{m}^3$ with and without zonal flows. Average values of σ are used for discussions. Findings reveal $l_{cr} \propto M_i^{0.11}$, $l_{c\theta} \propto M_i^{0.53}$, and $\omega_c \propto M_i^{-0.76}$ close to $\omega_T \propto M_i^{-0.87}$ for cases with zonal

TABLE I. Predicted isotope scaling exponent σ in comparison with empirical scalings.

	gKPSP simulator		ASDEX		ITER89-P L-mode	ITER-IPB98(y) H-mode
	LOC	SOC	LOC	SOC		
σ	0.5	0.25	0.31	0.5	0.5	0.2

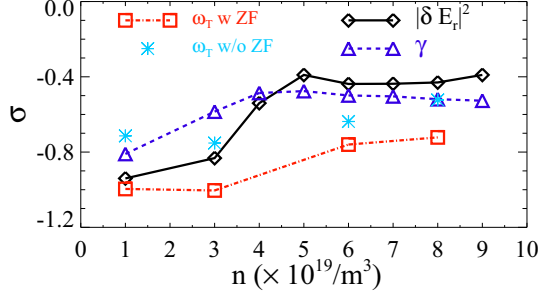


FIG. 4. σ for turbulence radial electric field intensity $|\delta E_r|^2$ (black), linear growth rate γ (blue), eddy turnover rates ω_T with (red) and without (gray) zonal flow as a function of density.

flow. Scalings of ω_c or ω_T with M_i starkly contrast with characteristic linear frequency $\omega_{*e} \propto c_s/a \propto M_i^{-0.5}$.

From mixing length estimations, energy confinement time is $\tau \propto 1/\chi \propto 1/l_c^2 \omega_c \propto M_i^{0.54}$ using the radial correlation length and $\tau \propto M_i^{-0.3}$ with the poloidal correlation length. Dimensional analysis suggests a more crucial role of radial electric field in isotope effects. Furthermore, $l_{cr} \propto M_i^{0.11}$ deviates significantly from the gyro-Bohm scaling which predicts $l_{cr} \propto M_i^{0.5}$. In contrast, $l_{c\theta} \propto M_i^{0.53}$ follows the gyro-Bohm scaling, implying anisotropic spatial isotopic dependence. Due to the crucial role of radial correlation, we performed convergence tests with regards to radial grid size and domain size for $n = 3.0 \times 10^{19} \text{ m}^{-3}$. In one test, we increase the radial grid number from $N_r = 288$ to $N_r = 432$. In the other one, ρ^{*-1} is doubled from 220 to 440, as we note $\rho^{*-1} > 500$ was adopted in recent gyrokinetic simulations of LOC-SOC transition [32]. Both tests show consistent isotopic dependence of radial correlation length, confirming the convergence. In addition, l_{cr} is more strongly influenced by the radial equilibrium scale length (radial domain size) than the isotope mass. In the case $a/\rho_{iH} = 220$, $l_{cr} = 8.64\rho_{iH}$, $9.55\rho_{iH}$ and $10.2\rho_{iH}$ for H, D, and T, respectively, with $l_{cr} \propto M_i^{0.15}$. In the other case $a/\rho_{iH} = 440$, $l_{cr} = 12.27\rho_{iH}$, $13.66\rho_{iH}$, and $14.61\rho_{iH}$ for H, D, and T, respectively, with $l_{cr} \propto M_i^{0.158}$. Obviously, this is one of the reasons why early attempts for explanation of isotopic dependence of confinement involved the trapped ion mode led to Bohm, rather than gyro-Bohm scaling [36]. Upon removing zonal flows, we find $l_{cr}^{(0)} \propto M_i^{0.10}$, $\omega_c^{(0)} \propto M_i^{-0.61}$, and $\tau^{(0)} \propto M_i^{0.41}$. Thus, zonal flow primarily enhances isotopic dependence of confinement by reinforcing the inverse dependence of decorrelation rate on isotopes. Results align with experimental measurements on DIII-D [10], validating the isotopic reduction of decorrelation rate.

We further classify contributors to isotope effects: deviation from gyro-Bohm scaling, zonal flow, and TEM stabilization. Scaling factors σ for $|\delta E_r|^2$, γ , and ω_T are showcased in Fig. 4. Firstly, the deviation from gyro-Bohm scaling is characterized by $l_{cr} \propto M_i^{0.11}$ and inherent isotopic dependence of $\gamma \propto M_i^{-0.5}$, identifiable in the ITG-dominant SOC regime. For example, with $n = 8.0 \times 10^{19} \text{ m}^{-3}$, $\gamma \propto M_i^{-0.5}$ aligns with $|\delta E_r|^2 \propto M_i^{-0.43}$, yielding $\chi \propto \gamma/\bar{k}_r^2 \propto M_i^{-0.28}$ from mixing length estimation. Secondly, TEM stabilization becomes clear in the TEM-dominant LOC regime, where $\gamma \propto$

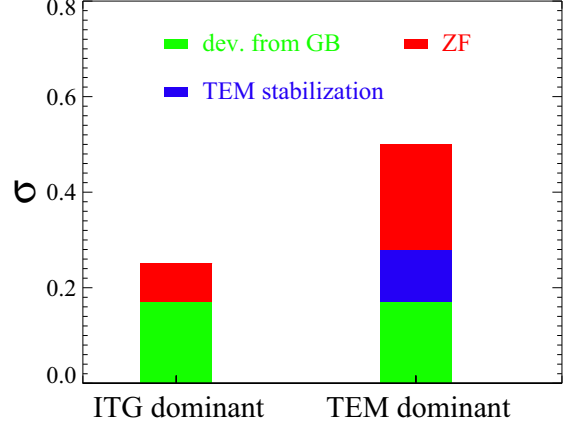


FIG. 5. Contributions to σ from participants: deviation from gyro-Bohm scaling (green), zonal flow (red) and TEM stabilization (blue) in ITG and TEM dominant regimes.

$M_i^{-0.8}$, in line with $|\delta E_r|^2 \propto M_i^{-0.94}$ for $n = 1.0 \times 10^{19} \text{ m}^{-3}$. Evidently, TEM stabilization amplifies isotope effects, adding to the deviation from gyro-Bohm scaling. This observation corroborates the findings presented in Refs. [13,15]. Thirdly, zonal flow adds to isotope effects by enhancing the inverse dependence of the decorrelation rate (turbulence eddy turn over rate) on isotopes, as illustrated in Fig. 4. Since $\omega_T \propto k_\theta k_r \delta\phi$ and $k_\theta \propto M_i^{-0.53}$, following the nature of microturbulence regardless of zonal flow presence, impacts of zonal flow come from the reinforcement of turbulence radial electric field mitigation by isotopes. This is confirmed as we find $k_r \delta\phi \propto M_i^{-0.34}$ with zonal flow and $k_r \delta\phi \propto M_i^{-0.17}$ without zonal flow. Figure 5 quantifies each contributor's impact in TEM- and ITG-dominant regimes. For this figure, we calculate the average σ for TEM- and ITG-dominant turbulence, with and without zonal flow, from Fig. 2.

It is worth noting that electron-ion collision ν_{ei} is independent of ion mass and remains a constant for isotopes. Understanding of the role of electron-ion collision in TEM stabilization by isotopes is nontrivial. A potential explanation can be inferred from TEM dispersion relation, which requires the resonance condition $\omega - \bar{\omega}_{de} + i\nu_{ei}/\varepsilon$ [37]. Given that $\omega - \bar{\omega}_{de} \propto M_i^{-0.5}$ and $\nu_{ei}/\varepsilon \propto M_i^0$, collisional broadening of wave-particle resonance for TEM drive is comparatively stronger for larger ion mass, resulting in weaker turbulence and diminished transport. Furthermore, electron-ion collision stabilizes TEM by detraping the trapped electrons. Detrapping rate f_{dt} , defined as percentage of detrapped electrons per unit time, emerges as a critical metric for evaluating detrapping effects [20]. Our simulations reveal that $f_{dt} \propto M_i^{0.6}$. This indicates that isotopes accelerate detrapping of trapped electrons and disrupt trapped electron ∇B drift resonance more rapidly, leading to TEM mitigation.

This study exemplifies the isotopic dependence of energy confinement, $\tau \propto M_i^\sigma$, with $\sigma \simeq 0.5$ in the low-density LOC regime and $\sigma \simeq 0.25$ in the high-density SOC regime. This finding aligns with empirical scalings with σ ranging from 0.2 to 0.5. Within this robust correlation, we identify a paramount

physical mechanism: mitigation of turbulence radial electric field energy $|\delta E_r|^2$ and correlated poloidal fluctuating $\delta \mathbf{E} \times \mathbf{B}$ flow, dictated by radial correlation length $l_{cr} \propto M_i^{0.11}$, that greatly diverges from gyro-Bohm scaling. Notably, impact of turbulence radial electric field and correlated poloidal fluctuating $\delta \mathbf{E} \times \mathbf{B}$ flow on transport and confinement remains a key focus for future research. Our findings suggest this aspect should receive considerable emphasis, offering a potential direction for experimental exploration and building a theoretical

foundation for isotope effects. This work may have significant implications for optimizing energy confinement in tokamak plasmas.

This work is supported by the R&D Program through Korea Institute of Fusion Energy (KFE) funded by the Ministry of Science, ICT and Future Planning of the Republic of Korea (KFE-EN2341-9). Simulations were run on the KFE KAIROS supercomputer.

-
- [1] B. Bigot, Progress toward ITER's first plasma, *Nucl. Fusion* **59**, 112001 (2019).
- [2] M. Bessenrodt-Weberpals, F. Wagner, O. Gehre, L. Giannone, J. V. Hofmann, A. Kallenbach, K. McCormick, V. Mertens, H. D. Murmann, F. Ryter, B. D. Scott, G. Siller, F. X. Soldner, A. Stabler, K.-H. Steuer, U. Stroth, N. Tsois, H. Verbeek, and H. Zoehm, The isotope effect in ASDEX, *Nucl. Fusion* **33**, 1205 (1993).
- [3] F. Wagner and U. Stroth, Transport in toroidal devices – The experimentalist's view, *Plasma Phys. Control. Fusion* **35**, 1321 (1993).
- [4] M. Wakatani, V. S. Mukhovatov, K. H. Burrell, J. W. Connor, J. G. Cordey, Yu. V. Esipchuk, X. Garbet, S. V. Lebedev, M. Mori, K. Toi, and S. M. Wolfe, ITER Physics Expert Group on Confinement and Transport, Plasma confinement and transport, *Nucl. Fusion* **39**, 2175 (1999).
- [5] J. G. Cordey, B. Balet, D. V. Bartlett, R. V. Budny, J. P. Christiansen, G. D. Conway, L.-G. Eriksson, G. M. Fishpool, C. W. Gowers, J. C. M. de Haas, P. J. Harbour, L. D. Horton, A. C. Howman, J. Jacquinot, W. Kerner, C. G. Lowry, R. D. Monk, P. Nielsen, E. Righi, F. G. Rimini *et al.*, Plasma confinement in JET H mode plasmas with H, D, DT and T isotopes, *Nucl. Fusion* **39**, 301 (1999).
- [6] H. Urano, T. Takizuka, M. Kikuchi, T. Nakano, N. Hayashi, N. Oyama, and Y. Kamada, Small ion-temperature-gradient scale length and reduced heat diffusivity at large hydrogen isotope mass in conventional H-mode plasmas, *Phys. Rev. Lett.* **109**, 125001 (2012).
- [7] P. A. Schneider, P. Hennequin, N. Bonanomi, M. Dunne, G. D. Conway, U. Plank, the ASDEX Upgrade Team, and the EUROfusion MST1 Team, Overview of the isotope effects in the ASDEX Upgrade tokamak, *Plasma Phys. Control. Fusion* **63**, 064006 (2021).
- [8] K. Ida, Isotope effect of transport and key physics in the isotope mixture plasmas, *Rev. Mod. Plasma Phys.* **7**, 23 (2023).
- [9] P. N. Yushmanov, T. Takizuka, K. S. Riedel, O. J. W. F. Kardaun, J. G. Cordey, S. M. Kaye, and D. E. Post, Scalings for tokamak energy confinement, *Nucl. Fusion* **30**, 1999 (1990).
- [10] Z. Yan, P. Gohil, G. R. McKee, D. Eldon, B. Grierson, T. Rhodes, and C. C. Petty, Turbulence and sheared flow structures behind the isotopic dependence of the L-H power threshold on DIII-D, *Nucl. Fusion* **57**, 126015 (2017).
- [11] C. F. Maggi, H. Weisen, F. J. Casson, F. Auriemma, R. Lorenzini, H. Nordman, E. Delabie, F. Eriksson, J. Flanagan, D. Keeling, D. King, L. Horvath, S. Menmuir, A. Salmi, G. Sips, T. Tala, I. Voitsekhovich, and JET Contributors, Isotope identity experiments in JET-ILW with H and D L-mode plasmas, *Nucl. Fusion* **59**, 076028 (2019).
- [12] Y. Xu, C. Hidalgo, I. Shestrikov, A. Krämer-Flecken, S. Zoletnik, M. Van Schoor, M. Vergote, and the TEXTOR Team, Isotope effect and multiscale physics in fusion plasmas, *Phys. Rev. Lett.* **110**, 265005 (2013).
- [13] M. Nakata, M. Nunami, H. Sugama, and T. H. Watanabe, Isotope effects on trapped-electron-mode driven turbulence and zonal flows in helical and tokamak plasmas, *Phys. Rev. Lett.* **118**, 165002 (2017).
- [14] J. Garcia, T. Görler, F. Jenko, and G. Giruzzi, Gyrokinetic nonlinear isotope effects in tokamak plasmas, *Nucl. Fusion* **57**, 014007 (2017).
- [15] I. Pusztai, J. Candy, and P. Gohil, Isotope mass and charge effects in tokamak plasmas, *Phys. Plasmas* **18**, 122501 (2011).
- [16] T. S. Hahm, Lu Wang, W. X. Wang, E. S. Yoon, and F. X. Duthoit, Isotopic dependence of residual zonal flows, *Nucl. Fusion* **53**, 072002 (2013).
- [17] A. Bustos, A. Bañón Navarro, T. Görler, F. Jenko, and C. Hidalgo, Microturbulence study of the isotope effect, *Phys. Plasmas* **22**, 012305 (2015).
- [18] E. A. Belli, J. Candy, and R. E. Waltz, Reversal of simple hydrogenic isotope scaling laws in tokamak edge turbulence, *Phys. Rev. Lett.* **125**, 015001 (2020).
- [19] Y. Idomura, Isotope and plasma size scaling in ion temperature gradient driven turbulence, *Phys. Plasmas* **26**, 120703 (2019).
- [20] L. Qi, J.-M. Kwon, H. Jhang, T. S. Hahm, and M. Leconte, Nonlinear gyrokinetic analysis of linear ohmic confinement to saturated ohmic confinement transition, *Nucl. Fusion* **60**, 036009 (2020).
- [21] E. Delabie, M. F. F. Nave, P. Rodriguez-Fernandez, B. Lomanowski, M. Baruzzo, T. M. Biewer, J. Garcia, J. C. Hillesheim, N. T. Howard, D. King, M. Lennholm, D. Kos, C. F. Maggi, H. J. Sun, and JET Contributors, The isotope effect on core heat transport in JET-ILW ohmic plasmas in hydrogen, deuterium and tritium, 29th IAEA-FEC Conference (London, 2023).
- [22] D. V. Kouprienko, A. D. Gurchenko, E. Z. Gusakov, A. B. Altukhov, L. G. Askinazi, A. A. Belokurov, V. V. Dyachenko, L. A. Esipov, V. A. Ivanov, O. A. Kaledina, S. I. Lashkul, S. V. Shatalin, A. V. Sidorov, N. V. Tropin, and S. Janhunen, Isotope effect in turbulent transport in high density FT-2 tokamak discharges, *Nucl. Fusion* **62**, 066045 (2022).
- [23] K. Tanaka, O. Krutkin, S. Coda, F. Bagnato, A. Perek, A. Karpushov, D. Mykytchuk, B. Labit, L. Martinelli, H. Weisen, O. Sauter, B. P. Duval, and B. L. Linehan, Isotope effects

- of multiple transport channels in TCV Ohmic discharge, 29th IAEA-FEC conference (London, UK, 2023).
- [24] T. S. Hahm, Nonlinear gyrokinetic equations for tokamak microturbulence, *Phys. Fluids* **31**, 2670 (1988)
 - [25] A. Brizard, Nonlinear gyrokinetic Maxwell-Vlasov equations using magnetic coordinates, *J. Plasma Phys.* **41**, 541 (1989).
 - [26] B. H. Fong and T. S. Hahm, Bounce-averaged kinetic equations and neoclassical polarization density, *Phys. Plasmas* **6**, 188 (1999).
 - [27] L. Qi, J.-M. Kwon, T. S. Hahm, and G. Jo, Gyrokinetic simulations of electrostatic microinstabilities with bounce-averaged kinetic electrons for shaped tokamak plasmas, *Phys. Plasmas* **23**, 062513 (2016).
 - [28] J. M. Kwon, L. Qi, S. Yi, and T. S. Hahm, ITG–TEM turbulence simulation with bounce-averaged kinetic electrons in tokamak geometry, *Comput. Phys. Commun.* **215**, 81-90 (2017).
 - [29] L. Qi, J.-M. Kwon, T. S. Hahm, and S. Yi, Bounce-averaged gyrokinetic simulation of trapped electron turbulence in elongated tokamak plasmas, *Nucl. Fusion* **57**, 124002 (2017).
 - [30] L. Qi, M. J. Choi, M. Leconte, T. S. Hahm, and J. M. Kwon, Global $\mathbf{E} \times \mathbf{B}$ flow pattern formation and saturation, *Nucl. Fusion* **62**, 126025 (2022).
 - [31] J. Citrin, H. Arnichand, J. Bernardo, C. Bourdelle, X. Garbet, F. Jenko, S. Hacquin, M. J. Pueschel, and R. Sabot, Comparison between measured and predicted turbulence frequency spectra in ITG and TEM regimes, *Plasma Phys. Control. Fusion* **59**, 064010 (2017).
 - [32] Y. Idomura, G. Dif-Pradalier, X. Garbet, Y. Sarazin, and Tore Supra Team, Full- f gyrokinetic simulations of Ohmic L-mode plasmas in linear and saturated Ohmic confinement regimes, *Phys. Plasmas* **30**, 042508 (2023).
 - [33] H. Chen and L. Chen, On the cascading of collisionless trapped-electron mode turbulence in tokamak plasmas, *Nucl. Fusion* **59**, 074003 (2019).
 - [34] L. Qi, Energy transfer of trapped electron turbulence in tokamak fusion plasmas, *Sci. Rep.* **12**, 5042 (2022).
 - [35] H. Chen and L. Chen, How zonal flow affects trapped-electron-driven turbulence in tokamak plasmas, *Phys. Rev. Lett.* **128**, 025003 (2022).
 - [36] T. S. Hahm and W. M. Tang, Nonlinear theory of collisionless trapped ion modes, *Phys. Plasmas* **3**, 242 (1996).
 - [37] J. C. Adam, W. M. Tang, and P. H. Rutherford, Destabilization of the trapped-electron mode by magnetic curvature drift resonances, *Phys. Fluids* **19**, 561 (1976).